

# Magneto photoluminescence measurements of tungsten disulphide monolayers

Jan Kuhnert,<sup>1</sup> Arash Rahimi-Iman,<sup>1</sup> and Wolfram Heimbrodt<sup>1, a)</sup>

*Faculty of Physics and Materials Sciences Center, Philipps-University 35032 Marburg, Germany*

(Dated: 30 September 2016)

Layered transition-metal dichalcogenides have attracted great interest in the last few years. Thinned down to the monolayer limit they change from an indirect band structure to a direct band gap in the visible region. Due to the monolayer thickness the inversion symmetry of the crystal is broken and spin and valley are coupled to each other. The degeneracy between the two equivalent valleys, K and K', respectively, can be lifted by applying an external magnetic field. Here, we present photoluminescence measurements of CVD-grown tungsten disulphide (WS<sub>2</sub>) monolayers at temperatures of 2 K. By applying magnetic fields up to 7 T in Faraday geometry, a splitting of the photoluminescence peaks can be observed. The magnetic field dependence of the A-exciton, the trion and three bound exciton states is discussed and the corresponding g-factors are determined.

## I. INTRODUCTION

In the last few years, a new class of monolayer materials has emerged after the successful rise of graphene: transition metal dichalcogenides (TMDCs). The most popular representatives are MoS<sub>2</sub>, MoSe<sub>2</sub>, WS<sub>2</sub>, and WSe<sub>2</sub>. They have attracted great interest from physicists all over the world due to their outstanding physical properties<sup>1–6</sup>. Thinned down to single layers, they change from an indirect band gap semiconductor in the bulk to a direct band gap semiconductor in the monolayer regime with its direct band gap located in the K and K' valley of the Brillouin zone<sup>7,8</sup>. The optical properties of these materials have already been widely studied. One very interesting aspect, to name but a few, is that in the monolayer limit the spin and valley degrees of freedom are coupled. This allows to selectively address the K or the K' valley by the helicity of the incident light<sup>9–12</sup>. To break the degeneracy of the energetically equivalent K and K' valleys, an external magnetic field can be applied that couples to the magnetic moments perpendicular to the hexagonal lattice structure of each valley. Due to the different sign of the magnetic moments in the K and K' valley, the two components split into two Zeeman components which spectrally can be distinguished. Up to now investigations on the magnetic properties of transition metal diselenides have been reported<sup>9,10,13–16</sup>.

So far, the excitonic g-factors for monolayers have been determined for neutral excitons (A exciton) to be  $(-3.94 \pm 0.04)$  in WS<sub>2</sub><sup>17</sup>,  $(-4.0 \pm 0.2)$  in MoS<sub>2</sub><sup>17</sup>,  $(-3.7 \pm 0.2)$ ,  $(-4.37 \pm 0.15)$ ,  $(-4.0 \pm 0.5)$ ,  $(-1.57 \text{ upto } -2.86)$  in WSe<sub>2</sub><sup>13–15,18</sup>, and  $(-3.8 \pm 0.2)$ <sup>10,18</sup> and  $(-4.1 \pm 0.2)$ <sup>9</sup> in MoSe<sub>2</sub>, respectively. Reported values for the g-factor of the second excitonic transition (B exciton) are only available for bulk material:  $(-3.99 \pm 0.04)$  for WS<sub>2</sub> and  $(-4.65 \pm 0.17)$  for MoS<sub>2</sub><sup>17</sup>. For charged excitons (tri-

ons) in WSe<sub>2</sub> effective g-factors of  $(-4.0 \pm 0.5)$  and  $(-6.28 \pm 0.32)$ <sup>14,15</sup> are reported, and for MoSe<sub>2</sub> g-factors of  $(-3.8 \pm 0.2)$ <sup>10</sup> and  $(-4.1 \pm 0.2)$  upto  $(-6.2 \pm 0.2)$  depending on the doping level<sup>9</sup> are reported, respectively. To our knowledge there have been no reports on trionic g-factors for transition metal disulphides yet.

It is worth to note that the photoluminescence (PL) of the TMDCs, however, often consists of various bands: Besides the A-exciton and trion, the bi-exciton and even bound exciton states can be observed, which can show a similar but yet not identical behaviour in external fields. In this work we perform polarization-resolved PL measurements of WS<sub>2</sub> monolayers in magnetic fields up to 7 T, in order to determine the g-factors of these various excitonic species in this host lattice.

## II. MATERIALS & METHODS

### A. Sample

The WS<sub>2</sub> monolayer sample was grown via CVD on an opaque silicon substrate covered by SiO<sub>2</sub>. The substrate size is approximately  $20 \times 10 \text{ mm}^2$  and was purchased from 2Dsemiconductors Inc. The WS<sub>2</sub> monolayers are triangularly shaped and have a size of roughly  $30 \times 30 \text{ }\mu\text{m}^2$ .

### B. Raman measurements

To find the monolayer flakes on the sample raman measurements were performed prior to measuring the magneto PL. The raman measurements were carried out at room temperature using a standard Olympus BX41 microscope equipped with a raman setup. A 80 mW small band 514.5 nm argon-ion laser was focused on the sample via a 100x standard objective. The holographic notch filter allows to measure raman shifts bigger than  $200 \text{ cm}^{-1}$  relative to the laser wavenumber which is sufficient to

<sup>a)</sup> Electronic mail: Wolfram.Heimbrodt@physik.uni-marburg.de

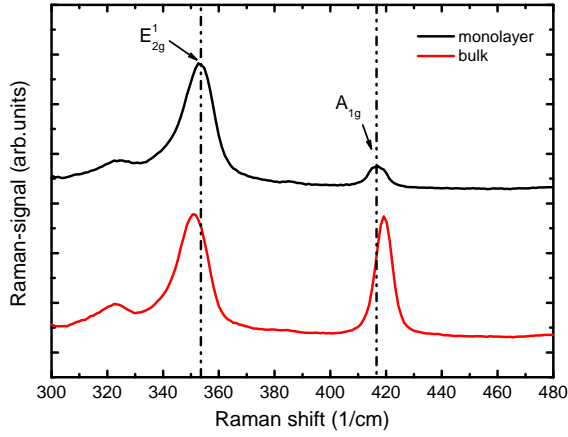


FIG. 1. Raman measurement of the  $\text{WS}_2$  sample with the characteristic  $A_{1g}$  and  $E_{2g}^1$  raman lines. The smaller energy difference for the monolayer mode ( $63.46 \text{ cm}^{-1}$ ) can be clearly seen compared to the bulk mode ( $68 \text{ cm}^{-1}$ ). The experiments were carried out at room temperature.

measure the characteristic  $A_{1g}$  and  $E_{2g}^1$  raman lines at  $\sim 420$  &  $350 \text{ cm}^{-1}$ , respectively.

### C. Magneto luminescence measurements

For the magneto-PL (M-PL) measurements, the sample was glued into an Oxford cryostat that is equipped with a superconducting liquid helium cooled magnet delivering fields up to 7 Tesla. The fields can either be applied in Voigt or in Faraday geometry. For our measurements, we solely used the Faraday geometry, for which the applied magnetic field is parallel to the  $k$ -vector of the emitted light field and therefore perpendicular to the sample surface. The sample was excited by a 150 mW 532 nm diode-pumped intracavity-frequency-doubled Nd:YAG laser, which was focussed onto the sample via a lens to a spot size of approximately  $25 \times 25 \mu\text{m}^2$ . PL was collected, collimated and focussed via lenses onto the 10  $\mu\text{m}$  entrance slit of a 1250 mm spectrometer equipped with a 1200-lines grating and detected by a highly sensitive thermo-electrically-cooled silicon CCD. In order to distinguish between  $\sigma^+$ - and  $\sigma^-$ -polarized light, a linear-polarizer plate was placed in front of the entrance slit of the spectrometer and a rotateable quarter-wave plate in front of the polarizer to select the desired circular polarization. All measurement were carried out at a sample temperature of 2 K.

## III. RESULTS & DISCUSSION

Raman spectroscopy is an excellent tool to identify the number of layers in few-layer TMDC flakes. Figure 1 displays typical Raman-spectra of such samples. Here, the

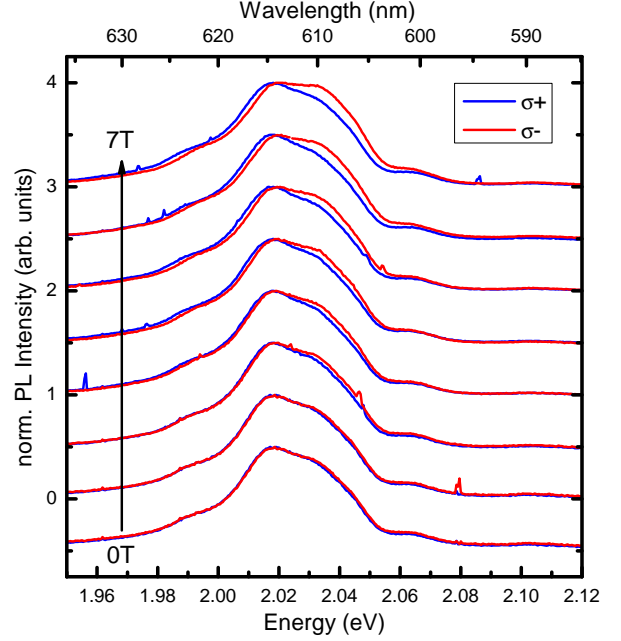


FIG. 2. Photoluminescence measurements of the  $\text{WS}_2$  monolayer with applied magnetic fields up to 7 Tesla in Faraday geometry using a 532 nm laser for excitation. The PL is detected in a  $\sigma^+$ - and  $\sigma^-$ -polarized basis. The sample temperature was kept at 2 K. The spectra are normalized and shifted vertically for clarity.

Raman signal of bulk  $\text{WS}_2$  is compared with the one from our CVD sample, both recorded at room temperature. The  $A_{1g}$  line, which is the out of plane mode, is located at  $416.70 \text{ cm}^{-1}$  and the  $E_{2g}^1$  line, the inplane mode, is located at  $353.24 \text{ cm}^{-1}$  in case of the CVD sample, respectively. The difference between both modes (indicated by dashed vertical lines in the diagram) is  $63.46 \text{ cm}^{-1}$  which is a good indicator for a monolayer regime. The respective separation in the case of the bulk sample is  $68 \text{ cm}^{-1}$ . The spectra are normalized to the  $E_{2g}^1$  line for the sake of clarity. The observed change in the relative separation ratio has been reported<sup>19</sup> and has been attributed to dielectric screening<sup>20</sup>.

The M-PL measurements at a temperature of 2 K are shown in figure 2 for left-circularly ( $\sigma^-$ , red solid lines) and right-circularly polarized ( $\sigma^+$ , blue solid lines) luminescence following laser excitation at 2.33 eV. The pump density amounted to  $15 \text{ kW cm}^{-2}$ . The spectra are normalized and offset by a constant value to form a waterfall diagram. The increasing splitting of the PL peaks with increasing magnetic field strength is clearly visible, here.

It is also apparent that with increasing fields the  $\sigma^-$ -component grows relative to the  $\sigma^+$ -component, becoming more pronounced on the higher-energy side of its peak.

It is obvious that the obtained spectrum is governed by an overlap of various bands. To get a deeper insight in the individual PL bands our representative spec-

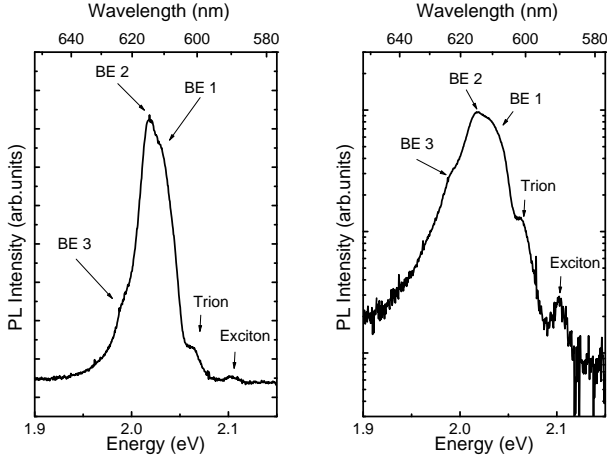


FIG. 3. Photoluminescence spectrum of the  $\text{WS}_2$  monolayer sample (linear plot on the left and logarithmic plot on the right hand side) at a temperature of 2 K without applied magnetic field. The logarithmic plot provides a more distinct view of the exciton and trion peaks.

trum is plotted both in linear (left) and logarithmic scale (right) in figure 3. We denote the individual peaks as generally accepted. The highest-energetic peak at 2.1 eV is assigned to the exciton in agreement with earlier papers<sup>21,22</sup>, where the exciton was found at 2.09 eV at a temperature of 5 K. The trion emission peak is centered at 2.06 eV. The visibility of the exciton and trion peaks at elevated energies indicates a high quality of the CVD sample, as this peak is absent in some earlier studies<sup>23,24</sup>. The most intense PL contribution (centered at 2.025 eV) stems from a superposition of three bands which we ascribe to bound exciton transitions (labeled BE1, BE2 and BE3). By applying a magnetic field in Faraday geometry, the  $\sigma^-$ -component shifts towards higher energies, while the  $\sigma^+$ -component is shifted to lower energies. Exemplarily, we show the spectra for the highest applied field of 7 T in  $\sigma^-$  (top) and  $\sigma^+$  (bottom) circular polarization in figure 4. To determine the effective g-factors of all the peaks, the spectra have been fitted by means of multiple gaussian shaped curves. One gaussian curve is used for each peak component, i.e. exciton, trion, defect-bound exciton 1,2,3, respectively.

Firstly, the PL spectrum in the case of zero external magnetic field was fitted with five gaussians to determine both the energetic positions and the full width at half maximum (FWHM) values. The exciton and trion peaks exhibits a substantially smaller FWHM (16.95 meV and 18.84 meV) than the defect-bound exciton-emissions (23.19 meV, 22.37 meV, and 21.38 meV). The FWHMs were kept unchanged for the fitting procedure in higher fields to reduce the number of free parameters. By fitting the  $\sigma^-$  and  $\sigma^+$  7 T spectra, we could determine the peak positions and amplitudes of the five bands. The best fitting results for both 7 T  $\sigma^-$  (top) and 7 T  $\sigma^+$  (bottom) are shown in figure 4. It should be mentioned that the

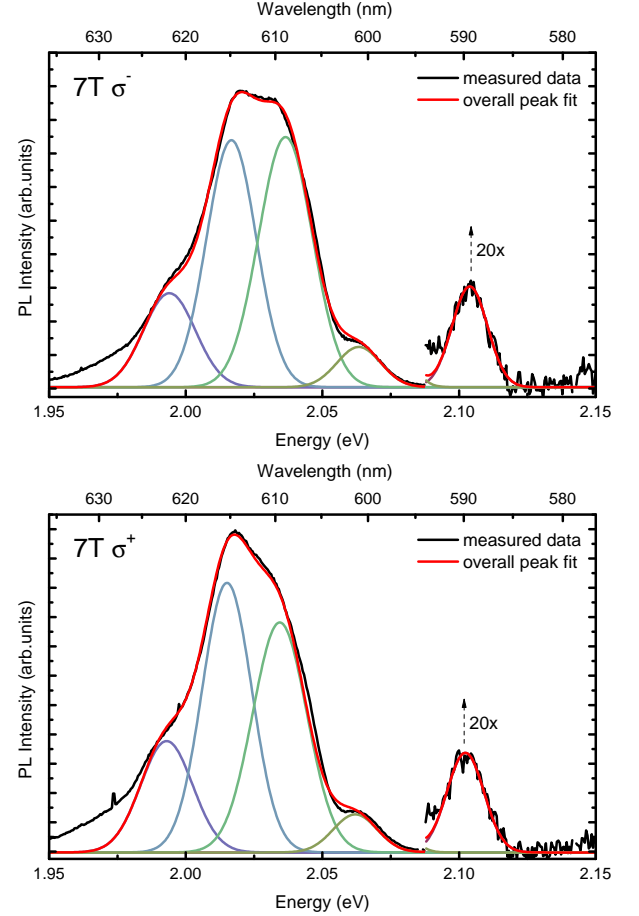


FIG. 4. Photoluminescence of the  $\text{WS}_2$  monolayer with applied magnetic field of 7 T for detection of  $\sigma^-$  (top) and  $\sigma^+$  (bottom) polarization of light. The peak components are fitted by using gaussian curves.

diamagnetic shift of the transitions does not need to be taken into account in a field range up to 7 T for these materials. Higher fields in the region of 50 to 100 T are needed for remarkable effects<sup>17</sup>.

The Zeeman splitting is given by the absolute difference between  $\sigma^-$  and  $\sigma^+$  of the center positions of the gaussian peaks for each individual species. Accordingly, for the excitonic transition we found a splitting per Tesla of  $22.86 \mu\text{eV T}^{-1}$ . The corresponding g-factor for the excitonic mode can be obtained by the equation:

$$g = \frac{2(E_+ - E_-)}{\mu_B B},$$

Here,  $g_{\text{exc}} = -3.95$  is in good agreement with previously reported values for  $\text{WS}_2$ <sup>17</sup>. For the trion peak, we got a total splitting of  $23 \mu\text{eV T}^{-1}$  with the resulting g-factor of  $g_{\text{trion}} = -3.97$  very close to the free exciton value. An identical value for excitons and trions has been reported also for the selenides<sup>9,10,14,15</sup>. Basically a very similar or identical value can be expected for excitons and trions, since the splitting arises mainly due to the difference in

the orbital magnetic moment of the initial and the final state. The spin contribution is expected to be zero, since the optical transitions take place between bands having the same spin. It should be mentioned, that there are also reports about a slightly higher g-value<sup>13,14</sup> for the trion.

It is interesting to note, that the three bound exciton states exhibit different g-values. We find a splitting of  $25.29 \mu\text{eV T}^{-1}$  for the BE1 centered at  $2.035 \text{ eV}$  which gives a g-factor of  $g_{\text{BE1}} = -4.37$ . This value is slightly higher than the values for the free exciton transition. The second bound exciton-emission peak (BE2) centered at  $2.0159 \text{ eV}$  shows a shift of  $23.14 \mu\text{eV T}^{-1}$  yielding a g-factors of  $g_{\text{BE2}} = -4.00$  in agreement with the free exciton value but the third band (BE3) centered at  $1.9935 \text{ eV}$  exhibits  $14.28 \mu\text{eV T}^{-1}$  with  $g_{\text{BE3}} = -2.47$ . The accuracy for the estimation of the g-factors is  $\pm 0.4$  in our analysis, mainly caused by the uncertainty of the gaussian peak determination. A different splitting for different sample positions, as mentioned in Ref<sup>13</sup>, could not be observed in our CVD grown sample. Our results strongly indicate a tendency: lower emission energies of the bound excitons are due to larger binding energies to the defect, which are most likely neutral or ionised donor or acceptor states. Larger binding energies and respective stronger localization of the excitons yield obviously smaller g-values. We ascribe these changes to different valley orbital contributions to the magnetic moments of the conduction and valence band. The simple two-band  $k \cdot p$  approximation with  $m_e = m_h$  does not affect the transition energies. Corrections beyond the two-band model give different effective masses and respectively different valley magnetic moments for the electrons and holes<sup>25,26</sup>.

#### IV. CONCLUSION

To summarize, we investigated the magneto-PL of CVD grown  $\text{WS}_2$  monolayers in magnetic fields up to 7 Tesla. In Faraday geometry, we revealed the Zeeman-splitting in polarization-sensitive spectra for five excitonic modes, the A-exciton, the trion and three bound exciton states. We determined the A-exciton g-factor to be  $g_{\text{exc}} = -3.95 \pm 0.4$ , the trion g-factor to be  $g_{\text{trion}} = -3.97 \pm 0.4$ . For the bound excitons we could determine deviations from the free exciton value, which should be caused by different effective masses of the electrons and holes due to different localization lengths.

#### ACKNOWLEDGMENTS

We gratefully acknowledge financial support of the German Science Foundation (DFG) in the framework of the SFB 1083. Furthermore, supply of high-quality samples for this study by 2Dsemiconductors Inc. is acknowl-

edged.

- <sup>1</sup>K. F. Mak, C. Lee, J. Hone, J. Shan, and T. F. Heinz, *Physical Review Letters* **105**, 136805 (2010), 1004.0546.
- <sup>2</sup>E. J. Sie, J. W. McIver, Y.-H. Lee, L. Fu, J. Kong, and N. Gedik, *Nature Materials* **14**, 290 (2015).
- <sup>3</sup>M. M. Ugeda, A. J. Bradley, S.-F. Shi, F. H. da Jornada, Y. Zhang, D. Y. Qiu, S.-K. Mo, Z. Hussain, Z.-X. Shen, F. Wang, S. G. Louie, and M. F. Crommie, *Nature materials* **13**, 1091 (2014), 1404.2331.
- <sup>4</sup>A. Chernikov, C. Ruppert, H. M. Hill, A. F. Rigosi, and T. F. Heinz, *Nature Photonics* **9**, 466 (2015).
- <sup>5</sup>W. Zhao, R. M. Ribeiro, M. Toh, A. Carvalho, C. Kloc, A. H. C. Neto, and G. Eda, *Nano Letters* **13**, 5627 (2013).
- <sup>6</sup>K. He, N. Kumar, L. Zhao, Z. Wang, K. F. Mak, H. Zhao, and J. Shan, *Phys. Rev. Lett.* **113**, 026803 (2014).
- <sup>7</sup>A. Splendiani, L. Sun, Y. Zhang, T. Li, J. Kim, C. Y. Chim, G. Galli, and F. Wang, *Nano Letters* **10**, 1271 (2010).
- <sup>8</sup>J. K. Ellis, M. J. Lucero, and G. E. Scuseria, *Applied Physics Letters* **99**, 261908 (2011).
- <sup>9</sup>Y. Li, J. Ludwig, T. Low, A. Chernikov, X. Cui, G. Arefe, Y. D. Kim, A. M. van der Zande, A. Rigosi, H. M. Hill, S. H. Kim, J. Hone, Z. Li, D. Smirnov, and T. F. Heinz, *Physical Review Letters* **113**, 1 (2014).
- <sup>10</sup>D. MacNeill, C. Heikes, K. F. Mak, Z. Anderson, A. Kormányos, V. Zólyomi, J. Park, and D. C. Ralph, *Physical Review Letters* **114**, 1 (2015).
- <sup>11</sup>T. Smoleński, M. Goryca, M. Koperski, C. Faugeras, T. Kazimierzczuk, A. Bogucki, K. Nogajewski, P. Kossacki, and M. Potemski, *Physical Review X* **6**, 021024 (2016).
- <sup>12</sup>T. Cao, G. Wang, W. Han, H. Ye, C. Zhu, J. Shi, Q. Niu, P. Tan, E. Wang, B. Liu, and J. Feng, *Nature Communications* **3**, 887 (2012), 1112.4013.
- <sup>13</sup>G. Aivazian, Z. Gong, a. M. Jones, R. L. Chu, J. Yan, D. G. Mandrus, C. Zhang, D. Cobden, W. Yao, and X. D. Xu, *Nature Physics* **11**, 148 (2015), 1407.2645.
- <sup>14</sup>A. Srivastava, M. Sidler, A. V. Allain, D. S. Lembke, A. Kis, and A. Imamoglu, *Nature Physics* **11**, 141 (2014), 1407.2624.
- <sup>15</sup>A. Mitoglu, P. P. Plochocka-Maude, A. Granados del Aguila, P. C. M. Christianen, G. Deligeorgis, S. Anghel, L. Kulyuk, and D. K. Maude, *Nano Letters* **15**, 4387 (2015).
- <sup>16</sup>A. A. Mitoglu, K. Galkowski, A. Surrente, L. Klopotoski, D. Dumcenco, A. Kis, D. K. Maude, and P. Plochocka, *Physical Review B* **93**, 165412 (2016).
- <sup>17</sup>A. V. Stier, K. M. McCreary, B. T. Jonker, J. Kono, and S. A. Crooker, *Nature Communications* **7**, 1 (2016), 1510.07022.
- <sup>18</sup>G. Wang, L. Bouet, M. M. Glazov, T. Amand, E. L. Ivchenko, E. Palleau, X. Marie, and B. Urbaszek, *2D Materials* **2**, 034002 (2015).
- <sup>19</sup>C. Lee, H. Yan, L. E. Brus, T. F. Heinz, J. Hone, and S. Ryu, *ACS Nano* **4**, 2695 (2010), 1005.2509.
- <sup>20</sup>A. Molina-Sánchez and L. Wirtz, *Physical Review B* **84**, 1 (2011), 1109.5499.
- <sup>21</sup>G. Plechinger, P. Nagler, J. Kraus, N. Paradiso, C. Strunk, C. Schüller, and T. Korn, *physica status solidi (RRL) - Rapid Research Letters* **9**, 457 (2015).
- <sup>22</sup>A. Chernikov, T. C. Berkelbach, H. M. Hill, A. Rigosi, Y. Li, O. B. Aslan, D. R. Reichman, M. S. Hybertsen, and T. F. Heinz, *Physical Review Letters* **113**, 076802 (2014).
- <sup>23</sup>A. A. Mitoglu, P. Plochocka, J. N. Jadczyk, W. Escoffier, G. L. J. a. Rikken, L. Kulyuk, and D. K. Maude, *Physical Review B - Condensed Matter and Materials Physics* **88**, 1 (2013).
- <sup>24</sup>G. Kioseoglou, M. Korkusinski, T. Scrase, A. T. Hanbicki, M. Currie, B. T. Jonker, and A. Petrou, *physica status solidi (RRL) - Rapid Research Letters* **9**, 1 (2015).
- <sup>25</sup>G.-B. Liu, W.-Y. Shan, Y. Yao, W. Yao, and D. Xiao, *Physical Review B* **88**, 085433 (2013).
- <sup>26</sup>A. Kormányos, V. Zólyomi, N. D. Drummond, P. Rakyta, G. Burkard, and V. I. Fal'ko, *Physical Review B - Condensed Matter and Materials Physics* **88**, 1 (2013).